Toxicology Letters 401 (2024) 125–138

Contents lists available at ScienceDirect

Toxicology Letters

journal homepage: www.journals.elsevier.com/toxicology-letters

Time-course characterization of whole-transcriptome dynamics of HepG2/C3A spheroids and its toxicological implications

Chanhee Kim [a], Zhaohan Zhu [b], W. Brad Barbazuk [c,d], Rhonda L. Bacher [b], Christopher D. Vulpe [a,*]

[a] Center for Human and Environmental Toxicology, Department of Physiological Sciences, College of Veterinary Medicine, University of Florida, Gainesville, FL, United States
[b] Department of Biostatistics, University of Florida, Gainesville, FL, United States
[c] Department of Biology, University of Florida, Gainesville, FL, United States
[d] University of Florida Genetics Institute, University of Florida, Gainesville, FL, United States

ARTICLE INFO

Editor : Dr. Angela Mally

Keywords:
3D cell culture
TempO-Seq
Gene expression
Metabolism
Cell proliferation

ABSTRACT

Physiologically relevant *in vitro* models are a priority in predictive toxicology to replace and/or reduce animal experiments. The compromised toxicant metabolism of many immortalized human liver cell lines grown as monolayers as compared to *in vivo* metabolism limits their physiological relevance. However, recent efforts to culture liver cells in a 3D environment, such as spheroids, to better mimic the *in vivo* conditions, may enhance the toxicant metabolism of human liver cell lines. In this study, we characterized the dynamic changes in the transcriptome of HepG2/C3A hepatocarcinoma cell spheroids maintained in a clinostat system (CelVivo) to gain insight into the metabolic capacity of this model as a function of spheroid size and culture time. We assessed morphological changes (size, necrotic core), cell health, and proliferation rate from initial spheroid seeding to 35 days of continuous culture in conjunction with a time-course (0, 3, 7, 10, 14, 21, 28 days) of the transcriptome (TempO-Seq, BioSpyder). The phenotypic characteristics of HepG2/C3A growing in spheroids were comparable to monolayer growth until ~Day 12 (Day 10–14) when a significant decrease in cell doubling rate was noted which was concurrent with down-regulation of cell proliferation and cell cycle pathways over this time period. Principal component analysis of the transcriptome data suggests that the Day 3, 7, and 10 spheroids are pronouncedly different from the Day 14, 21, and 28 spheroids in support of a biological transition time point during the long-term 3D spheroid cultures. The expression of genes encoding cellular components involved in toxicant metabolism and transport rapidly increased during the early time points of spheroids to peak at Day 7 or Day 10 as compared to monolayer cultures with a gradual decrease in expression with further culture, suggesting the most metabolically responsive time window for exposure studies. Overall, we provide baseline information on the cellular and molecular characterization, with a particular focus on toxicant metabolic capacity dynamics and cell growth, of HepG2/C3A 3D spheroid cultures over time.

1. Introduction

New approach methodologies (NAMs), including *in silico* and *in vitro* approaches, attempt to provide robust and cost-effective approaches to assess chemical hazards which simultaneously provide species appropriate, and targeted endpoint specific toxicity data while enabling reduced use or replacement of traditional animal models (Flecknell, 2002; Stokes, 2015; Zobl et al., 2023). Human *in vitro* models (Schmeisser et al., 2023) bypass the need for inter-species extrapolation (Lilienblum et al., 2008; Soldatow et al., 2012) (Singh et al., 2018) and may provide more relevant toxicity data than non-human models. Human *in vitro* liver cell models are widely used in toxicology and testing (Guillouzo, 1998; Soldatow et al., 2012; Mišík et al., 2019) as the human liver is both a major target organ of toxicity and a central player in toxicant metabolism and biotransformation. Currently, freshly isolated primary human hepatocytes (PHHs) represent the 'gold standard' in *in vitro* liver toxicity testing because of the preservation of central aspects of liver function including toxicant metabolism and responsiveness to

* Corresponding author.
E-mail address: cvulpe@ufl.edu (C.D. Vulpe).

https://doi.org/10.1016/j.toxlet.2024.10.004
Received 14 June 2024; Received in revised form 10 September 2024; Accepted 2 October 2024
Available online 3 October 2024
0378-4274/© 2024 The Authors. Published by Elsevier B.V. This is an open access article under the CC BY license (http://creativecommons.org/licenses/by/4.0/).

inducers (Bell et al., 2016; Yokoyama et al., 2018) but their availability, limited lifespan in commonly used culture systems, and heterogeneity limit their practical utility (Huggett et al., 2022). In contrast, immortalized liver cell lines, often derived from human tumors, provide homogenous cultures with unlimited lifespan (Wilkening et al., 2003), but generally lack comparable toxicant metabolic capacity and other cell type/tissue specific phenotypes when grown as a proliferating monolayer cultures (Pamies and Hartung, 2017). Indeed, the compromised metabolic capacity of the cell culture system used for pre-clinical toxicity studies may help to explain toxicity prediction failure and unexpected adverse outcomes in humans (Adams, 2019; Robinson et al., 2020). Thus, any NAM based on human cells must address the metabolic and phenotypic limitations of conventional monolayer cell culture.

Efforts to address the metabolic limitations of immortalized liver cell monolayer cultures include the addition of exogenous metabolic enzymes (Cox et al., 2016; Richardson et al., 2016; Deisenroth et al., 2020) new culture approaches (e.g. 3D cultures), development of new immortalized cell lines (e.g. HepaRG), or iPSC derived hepatocytes (Corbett and Duncan, 2019). A derivative of the HepG2 cell line, termed HepG2/C3A, has recently received increased interest as a possible model system with potentially enhanced metabolic capacity but its metabolic capability especially in 3D culture over extended culture times has not been adequately assessed (Ramaiahgari et al., 2014; Coltman et al., 2021). 3D culture approaches for liver cells range from relatively simple self-assembling spheroid models with a single cell type to complex scaffold-based approaches with multi-cellular organoids (Li et al., 2008; Haycock, 2011; Ramaiahgari et al., 2014; Štampar et al., 2019; Fontana et al., 2021). In general, these 3D models increase cell-cell and cell-matrix interactions, recover some liver-specific functions such as albumin content and urea synthesis, and increase expression of metabolizing enzymes (Wrzesinski et al., 2014). Continuously rotating 3D cell culture systems such as the ClinoStar system from CelVivo (Wrzesinski and Fey, 2013; Wrzesinski et al., 2013) that are based on the clinostat principle (free from unidirectional effects of gravity) are facilitating the formation of highly reproducible 3D structures (Wrzesinski and Fey, 2018). In this study, we utilize the ClinoStar system for a time course evaluation of long-term cultures of HepG2/C3A spheroids. Previous studies of the HepG2/C3A spheroids have focused on phenotypic endpoints (toxicity) (Wojdyla et al., 2016; Calitz et al., 2018; Štampar et al., 2021) or in the case of more comprehensive analysis (Frandsen et al., 2022, Stransky et al., 2022) considered only a limited time period of spheroid culture. While previous studies did examine alterations in mRNA expression of selected metabolically relevant genes (Eilenberger et al., 2019; Štampar et al., 2020, 2021; Coltman et al., 2021) in 3D spheroid culture, to our knowledge, the whole-transcriptomic landscape of the HepG2/CA3 spheroid hasn't been fully investigated and documented over time in clinostat culture. We used the TempO-Seq platform (BioSpyder™) (Bushel et al., 2018) which is widely used in high-throughput transcriptomics-based toxicology studies (Harrill et al., 2021; Rowan-Carroll et al., 2021; House et al., 2022) to characterize changes in the transcriptome of HepG2/C3A spheroids cultured in the ClinoStar system for up to 28 days to assess the long-term dynamics of cellular and transcriptional changes.

2. Materials and methods

2.1. HepG2/C3A 3D spheroid formation and maintenance

HepG2/C3A spheroids were generated according to a protocol provided by CelVivo (Wrzesinski and Fey, 2018; Wrzesinski et al., 2021; Frandsen et al., 2022). To generate uniformly sized spheroids, 500 cells/microwell (750 round-bottomed microwells/well) were seeded onto each well of the Spherical plate 5D (SP5D) 12-well plate (Kugelmeiers AG). After adding HepG2/C3A growth media (MEM media (Gibco) complemented with 1 % non-essential amino acids (Gibco) and 1 % Antibiotic-Antimycotic (Gibco)) up to a final volume of 2 ml per each well, the plate was centrifuged at 100xG for 3 min and incubated in a humidified incubator (Forma™ Series II Water-Jacketed CO2 Incubator, Thermo Scientific™) with 5 % CO_2 at 37 ∘C for 24 h to allow aggregation. Successful aggregation was determined by checking individual round-bottom microwells using a microscope (Nikon TMS). The ClinoReactors for spheroid propagation were prepared by hydration of the humidification beads inside the humidity chamber of the ClinoReactors with sterile water (CelVivo) for 4 h at room temperature Following chamber hydration, the ClinoReactors were filled with 5 ml of HepG2/C3A growth media and equilibrated overnight in ClinoStar (5 % CO_2 and 37 ∘C) rotating at 13 rpm. After equilibration, the media was removed from the ClinoReactors, and the pre-aggregated spheroids (~750 spheroids, all spheroids made from a single well of the SP5D plate) were gently transferred (Day 0) into the ClinoReactors using a transfer pipet (CelVivo). Spheroid-containing ClinoReactors were filled with the growth media to 10 ml and placed in ClinoStar under continuous rotation. Media was changed (90 % of the volume) two to three times a week and the rotation speed of each ClinoReactor was adjusted to ensure optimal media flow according to the increasing size of spheroids during culture, aiming that spheroids do not reach the top or bottom surface of the reactor. A "gardening" procedure was performed during media changes during which irregularly shaped/sized spheroids were removed to ensure spheroid uniformity. The ClinoReactor unit was replaced with a new ClinoReactor (replaced every 14 days) to ensure that cellular debris did not accumulate on the surfaces of the reactor. The HepG2/C3A spheroids were cultured for 35 days, and spheroid samples were harvested by collecting a portion of spheroids in the bioreactor for a variety of downstream phenotyping assays such as cell proliferation assays (1–3 spheroids depending on their size at each time point) and transcriptome profiling (3–20 spheroids depending on their size at each time point).

2.2. Imaging and monitoring of spheroid

Phase-contrast light microscopy images (4X and 10X magnification) of individual spheroids at each time point (from Day 1 to Day 35) were acquired using the BZ-X700 microscope (Keyence). Four replicates of the spheroids per time point were collected from ClinoReactors and transferred to 24-well tissue culture plate (Corning), and imaged. The BZ-X Analyzer software embedded within the BZ-X700 was used to analyze cell morphology parameters including area (μm^2), perimeter (μm), major axis (μm, length), minor axis (μm, width) of the spheroids. The average of major axis and minor axis was used as a proxy for diameter (μm) since a two-dimensional image of a spheroid is not perfectly circular.

2.3. Cell doubling time

Two cell growth parameters were measured in parallel (ATP-based cell proliferation assay and direct cell counting). For the cell proliferation assay, 10 replicates of spheroids per time point were assayed using the CellTiter-Glo 3D cell viability assay system (Promega) to produce relative light unit (RLU) values. For cell counting, 6 replicates of spheroids per each time point were dissociated to produce single cell suspension using Accutase solution (400–600 units/ml) (Sigma-Aldrich, A6964) and aliquot of the single cell suspension was cell-counted using CellDrop (DeNovix) with a dilution factor of 1–2. Peason correlation analysis via the CORREL function in excel (version 16.0) was performed to confirm correlation of cell growth parameters obtained from independent measurement. Next, cell doubling times were calculated according to the following equation:

$$Doubling = Duration\left(hour\right) \times \frac{\ln(2)}{\ln\left(\frac{Final\ cell\ growth\ parameter}{Initial\ cell\ growth\ parameter}\right)}$$

using RLU values of each time point as cell growth parameter. It is assumed that under cell culture conditions in this study cells proliferate at a constant speed, causing an exponential growth in cell number (Hirsch and Engelberg, 1965).

2.4. CYP enzymatic activity assay

We used the P450-Glo CYP3A4 assay with Luciferin-IPA substrate (Promega, Madison, WI) and the P450-Glo CYP1A1 assay with Luciferin-CEE (Promega, Madison, WI) to quantify enzymatic activities of CYP3A4 and CYP1A1 in 2D and 3D, respectively. Briefly, for detecting 2D enzymatic activities, 12,000 HepG2/C3A cells were seeded a day prior to the assay. Six spheroids were used per replicate for 3D spheroid at Day 3, 7, and 10. Both 2D and 3D spheroid samples were incubated with Luciferin-IPA (CYP3A4) and Luciferin-CEE (CYP1A1) for 3 h, followed by the addition of Luciferin detection reagent. After 20 min incubation at RT, the luminescence was measured. The enzymatic activities were normalized to ATP content measured by CellTiter-Glo 3D cell viability assay (Promega, Madison, WI). The assays were performed in three replicates.

2.5. TempO-Seq library preparation and next-generation sequencing

The whole-transcriptome of experimental HepG2/C3A cells was interrogated using the Human Whole Transcriptome Assay panel (BioSpyder Technologies Inc, Carlsbad, California) following the manufacturer's instructions for both monolayers and spheroids. Briefly, total RNA was extracted and purified from all experimental samples (3 replicates per sample) using a RNeasy Plus Mini Kit (Qiagen) following the manufacturer's instructions. Purified RNA samples were quantified, their 260/280 ratios assessed, and then diluted with sterile water to obtain a consistent concentration of 100 ng/μL across all samples. An equal volume of 2X TempO-Seq Enhanced Lysis Buffer was added to each RNA sample, which provides an assay-ready sample in 1X TempO-Seq Enhanced Lysis Buffer. The assay-ready samples were annealed to the detector oligo (DO, targeting and binding a single RNA of interest) mix using the following steps: the assay-ready samples were incubated on plate at 70°C for 10 minutes, then ramped to 45°C for 50 minutes with the same ramp rate; the plate was maintained at 45°C for 16 hours, then cooled to 25°C. Annealing was followed by nuclease digestion (37°C for 1.5 hours, the type of nuclease is not indicated by BioSpyder protocol) to remove excess oligos, and ligating (by incubating for 1 hour at 37°C, then immediately raise to 80°C for 15 minutes) of a pair of DOs. The ligated product was PCR amplified using primers that contain sample tag (index) sequences and adaptors required for sequencing using the following. PCR cycles: 1. 37°C for 10 minutes 2. 95°C for 1 minute 3. 25 cycles of 95°C 10 sec; 65°C 30 sec; 68°C 30 Section 4. 68°C for 60 Section 5. Hold at 25°C. The amplified assay products are then pooled and purified/concentrated using the Macherey-Nagel NucleoSpin Gel and PCR Cleanup kit (Takara Bio USA, Inc, Mountain View, California). The library was sequenced using a NovaSeqX (at BioSpyder). A median read depth of 1625 reads per gene was achieved.

Primary data analysis was performed on a raw fastq files by BioSpyder using the TempO-SeqR (v.3.0) program. Initially, reads were extracted from the bcl files and demultiplexed with bcl2fastq v.2.20.0.42. The fastq files were processed with the TempO-SeqR (v.3.0), which uses star v.2.5 to align the reads, and the count function from QuasR to extract feature counts using a gtf reference (Gaidatzis et al., 2015). A gene_count table that detailed the signal levels (counts) for each probe in each sample was provided.

2.6. Bioinformatics

All bioinformatics analyses for the TempO-Seq gene_count data were conducted using integrated Differential Expression and Pathway analysis version 1.13 (iDEPv1.13) (Ge et al., 2018). Counts were counts per million (CPM) normalized and genes without 0.5 CPM in at least one sample were removed from analysis. To facilitate clustering analyses and PCA the filtered gene count data were log2 transformed using the $\log_2$(cpm+c) function in the EdgeR package implemented in iDEPv1.13. To assess sample variability, Pearson correlations of the transformed cpm (i.e., $\log_2$(cpm+c)) were plotted to visually assess within sample similarity and between sample variability (Fig. S1).

2.6.1. Differentially expressed genes

iDEPv1.13 was used to perform differential gene expression analysis on all pairs of sample groups using the DESeq2(Love et al., 2014) R package implemented in iDEPv1.13. Expression was filtered at a fold-change > 2 and a false discovery rate (FDR) threshold of < 0.01. The resulting differentially expressed genes (DEGs) between comparison samples were then used to conduct enrichment analysis using Gene Ontology (Ensembl 92) and Kyoto Encyclopedia of Genes and Genomes (KEGG, Release 86.1) database.

2.6.2. Clustering analysis and Principal Component Analysis (PCA)

We applied a log transformation to the normalized gene expression counts to stabilize variance, followed by selecting the top 2000 genes based on standard deviation to focus on the most variable and informative genes. These selected genes were then Z-score standardized and K-means clustering was performed with the number of clusters set to four. We set $k = 4$ for the number of clusters based on the results of the elbow plot (Supplementary Fig. S2). Briefly, the elbow plot shows the within-cluster-sum-of-square (WCSS) values on the y-axis corresponding to the different values of K on the x-axis. The optimal k value is the point at which the graph forms an elbow.

2.6.3. Pathway enrichment analysis

2.6.3.1. Pathway enrichment analysis for DEGs: The analysis was done using fold-change values returned by DESeq2 implemented in iDEPv1.13 and R. For Fig. 5, selected genes involved in DNA replication and Cell cycle KEGG pathways underwent log transformation and Z-score normalization before generating the heatmaps.

2.6.3.2. Pathway enrichment analysis for clustered gene sets: Each cluster identified by k-means clustering as described above was analyzed for enriched pathways using gene sets derived from the GO-BP and KEGG databases implemented in iDEPv1.13 (accessed and performed Dec 3, 2023). The background genes used for the enrichment analysis are the filtered genes from the genome-wide original gene list. Enrichment p-values are calculated based on a one-sided hypergeometric test, which is then adjusted for multiple testing using the Benjamini-Hochberg procedure and converted to FDR. The pathways are first filtered based on an FDR threshold of 0.05, and then the significant pathways are sorted by FDR. Only the top 10 pathways are displayed.

2.6.4. Gene expression time-course dynamics

2.6.4.1. Data normalization. To account for variation in library size and sequencing depth across samples, we normalized the raw gene expression data using Median Normalization (Anders and Huber, 2010). Briefly, this method first calculates a 'size factor' for each sample accounting for variations in sequencing depth. Then, the method divides the expression values of each gene by the corresponding size factor. The result is a set of normalized expression values that are adjusted to a common scale across all samples.

2.6.4.2. Trendy analysis. To investigate the dynamics of gene expression over time, we employed the Trendy (Bacher et al., 2018) package in R, designed for analyzing high-throughput expression data (e.g., RNA-seq or microarray) across an ordered series of conditions, such as time-course experiments. Trendy identifies an optimal segmented regression model for each gene, with breakpoints indicate a significant

change in the gene's expression across the time-course. The lowest Bayesian Information Criterion (BIC) was selected for optimizing the segmented regression model for gene expression changes of each gene. Parameters were carefully chosen to balance sensitivity and specificity, with a maximum of three breakpoints, a minimum of five samples is required to be within a segment, and the p-value cutoff of 0.2 to identify significant changes in gene expression trends.

2.6.4.3. Toxicology genes of interest. The focused analysis used 39 genes associated with phase I, II, III drug and toxicant metabolism such as cytochrome P450 enzymes, glutathione transferases, and transporters. For each of these genes, we generated and displayed trendy plots to visualize the gene expression trends over time. The specific set of genes selected is presented in Table S2.

3. Results

3.1. Spheroid size continues to increase over 35 days of culture

Pre-aggregated HepG2/C3A 3D spheroids transferred into ClinoReactor (ClinoStar system, CelVivo) were maintained in continuous culture for up to 35 days. The size of the spheroids increased with the time of cultivation (Fig. 2A). The diameter of the spheroids was 228 μm on Day 1 and gradually increased to 348 μm on Day 7 (Fig. 2B). By Day 10, the diameter reached 570 μm, which is above the size (300–500 μm) previously shown to provide conditions resulting in lactate production, proliferation gradients, and hypoxia in HepG2/C3A cells (Wrzesinski and Fey, 2018; Pinto et al., 2020) similar to those observed in *in vivo* conditions. After Day 14, a darker region was noted in the center by imaging, consistent with a necrotic core (Zanoni et al., 2016; Barisam et al., 2018), distinct from the outer region (Fig. 2A). After 35 days of spheroid culture, the diameter of spheroids reached 1134 μm (Fig. 2B). The total area and perimeter of spheroids at each time point (Fig. S3A and S3B) increased in parallel with the diameter, confirming that HepG2/C3A 3D spheroids generated using the ClinoStar system continue to grow steadily over the long-term culture period of 35 days.

3.2. Individual cell proliferation rate decreases over time in spheroid culture

We investigated changes in the cellular growth rate of individual cells which make up the spheroids. Two methods, an ATP-based cell proliferation assay (CellTiter-Glo) and direct cell counting, were used to quantify the number of cells in each spheroid based on a random sample of each spheroid population at each time point. 10 spheroids were used for the cell proliferation assay and 6 spheroids were used for direct cell counting. A correlation analysis between RLU (Relative Light/Luminescence Unit) values resulting from the ATP-based cell proliferation assay and direct cell counts showed a statistically significant correlation between the two parameters, with a Pearson r value of 0.9762 and an R-square value of 0.953 (Fig. 2C) so RLU values were used to calculate the cell doubling time during the 35-day culture period compared to Day 1 (Fig. 2D). The cell doubling times in 3D spheroid culture increased over time to a maximum of 130 hours at 35 days compared to 40 hours observed in 2D monolayer. We noted a transition in doubling time around Day 14 of culture (i.e., from Day 10 to Day 21) with a 1.9 times increase in doubling time during subsequent culture times.

3.3. Whole-transcriptome profiling of HepG2/C3A time-course 3D culture using TempO-Seq platform reveals that formation and growth of spheroids accompanies extensive changes in gene expression

We used the TempO-Seq platform to comprehensively analyze whole-transcriptome changes (molecular phenotypic changes) of the HepG2/C3A spheroids over a time-course of culture as compared to 2D culture. First, Principal Component Analysis (PCA) was used to visualize data patterns and help identify samples with similar expression patterns and the variability in the gene expression across individual samples. PC1 (representing the largest variability in the data) and PC2 (representing the second largest variability in the data) account for 77 % and 18 % of variation, respectively (Fig. 3A). Biological replicates showed intra-sample consistency, and the analysis identified three distinct sample groups: 2D / Day 3, 7, and 10 / Day 14, 21, and 28 (Fig. 3A, Fig. S1). Furthermore, the 2D monolayer control samples are more distant from the other two groups than the other groups are from each other, which aligned with the result that a majority of DEGs were observed already by Day 3 (Table S1 and Fig. S7A). A large number of genes were found to be differentially expressed (DEGs_total range from 4816 to 5836 genes) throughout all the time points of spheroid culture compared to 2D monolayer controls (Table S1). A significant number of DEGs started to be differentially expressed as early as Day 3 (a total of 5767 genes, 2584 genes increased expression; 3183 genes decreased expression), which is nearly equivalent to the number of DEGs observed on Day 10 (a total of 5836 genes, 3277 genes increased expression; 2559 genes decreased

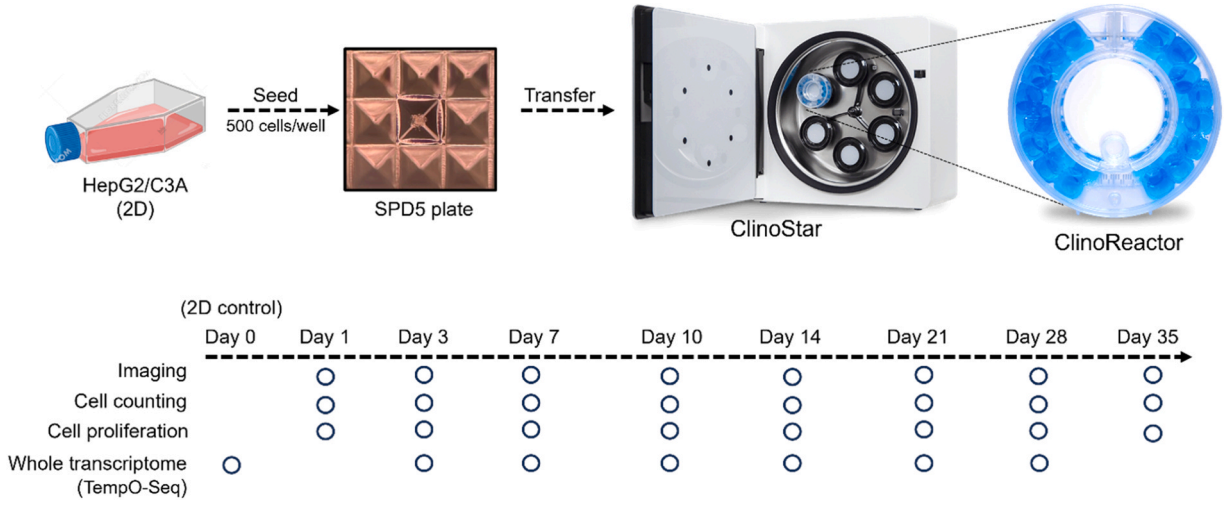


Fig. 1. Experimental scheme of this study. HepG2/C3A cells were originally cultured in 2D monolayer and subsequently seeded onto SPD5 ultra-low-attachment plate at a density of 500 cells/microwell for each single spheroid aggregate. Once the spheroid aggregates formed, they were transferred into a ClinoReactor rotating in a ClinoStar system (CelVivo) and cultured for up to 35 days. At the indicated timepoints, spheroid samples were characterized using Keyence microscope to determine spheroid size, dissociated to determine cell number and proliferation rate, and directly utilized for whole transcriptome analysis.

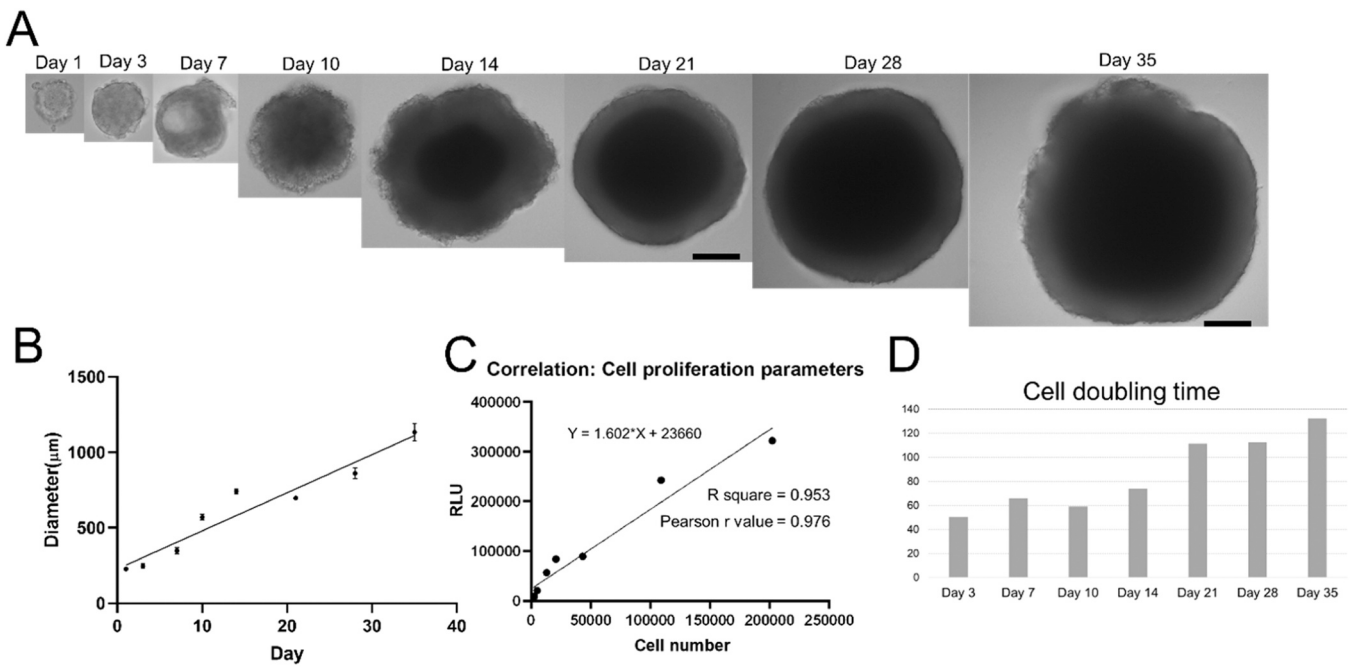


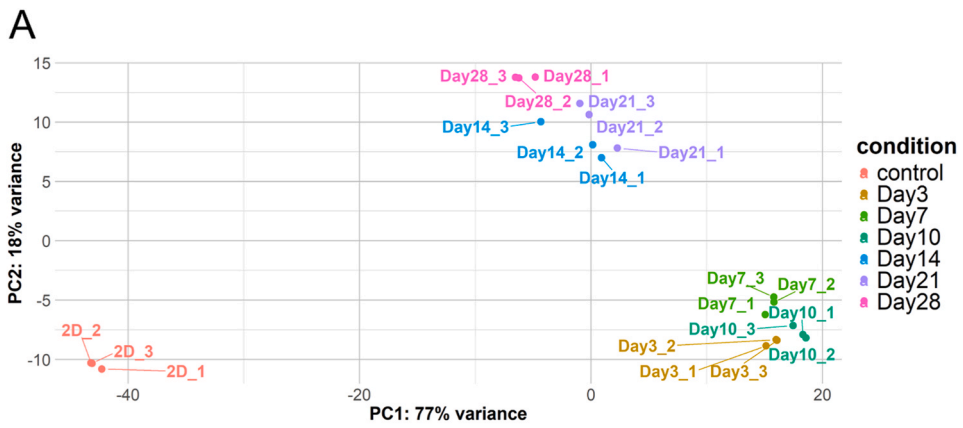
Fig. 2. Cellular phenotypic changes of HepG2/C3A spheroids over the time-course 3D culture. (A) Change in size of growing HepG2/C3A spheroids up to 35 days of cultivation in CelVivo clinostat-based bioreactors. The black scale bar indicates 200 μm. (B) Measured diameter (μm) of spheroids on each day of cultivation pictured in (A) is shown. (C) The result of correlation analysis of two cell proliferation (growth) parameters: cell number (x-axis) and relative light unit (RLU, y-axis) are plotted generating several correlation values. The equation of regression line is y=1.602*X + 23660, with R square of 0.953 and Pearson r value of 0.976. (D) Cell doubling times for each time points (x-axis) during 3D spheroid culture are shown as a bar graph. The units on the y-axis are hours.

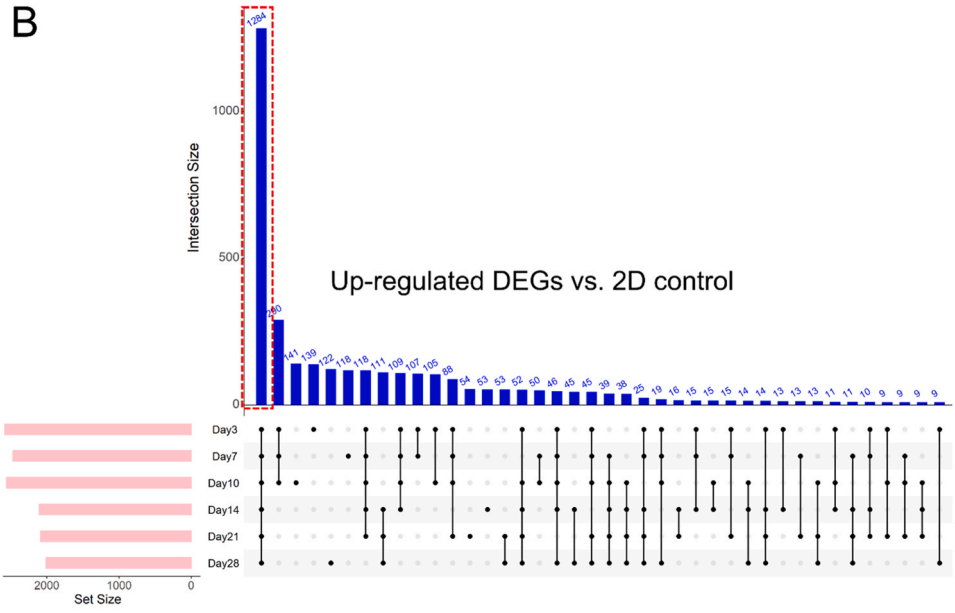
expression), representing the largest number of DEGs among all comparisons (Table S1). This result indicates that considerable changes in gene expression occurred rapidly (Day 3 or earlier) after formation of 3D spheroid structure. In addition, we identified 1284 genes found to be consistently differentially expressed across all time points (Fig. 3B). We assessed biological pathway enrichment (using GO terms) common to all time points in the 3D spheroid culture as compared to 2D culture and found that metabolism-related pathways such as small molecule metabolic process, oxoacid metabolic process, organic acid metabolic process, and carboxylic acid metabolic process are significantly enriched across all time points (Fig. 3C).

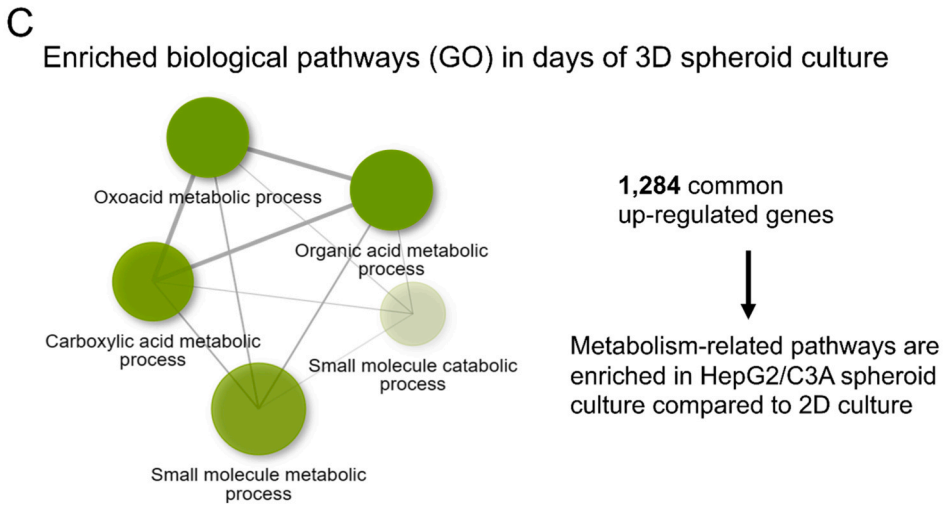
Since we noticed three distinct sample groups analyzed by PCA plot, we also assessed transcriptome changes over the time-course culture of spheroids by pair-wise comparisons of DEGs between adjacent time points (i.e., 2D vs. Day 3, Day 3 vs. Day 7, Day 7 vs. Day 10, Day 10 vs. Day 14, Day 14 vs. Day 21, Day 21 vs. Day 28) (Fig. S7) to see whether if the distinction of the time points was derived from a transcriptome change. Two main transitions of transcriptome dynamics were observed based on this analysis, which was supported by the result of the PCA plot (Fig. 3A). The first transition occurred during the change from 2D culture to 3D culture (Day 3) with 5666 DEGs (Fig. S7A), consistent with the finding that a substantial number of DEGs (enriched with metabolism-related genes and pathways) were observed by Day 3 and maintained throughout the spheroid cultures (Table S1). A second transition in gene expression was noted between Day 10 and Day 14 with 1406 DEGs (Fig. S7D), which involved DEGs other than the metabolism-related ones identified in the initial transition (Fig. S7A). In contrast, the direct comparisons of the other adjacent time points did not identify a large number of DEGs (Figs. S7B, S7C, S7E, and 4 F). In summary, the comparative analysis of DEGs between adjacent time points during the 3D spheroid culture revealed two transition time points where a substantial number of genes were differently expressed.

3.4. Clustering analysis captures patterns of transcriptome change during time-course 3D spheroid culture

Clustering analysis was performed to assess the changes in the transcriptome over the course of HepG2/C3A 3D spheroid culture. We carried out K-means clustering to further assess the changes in gene expression during the time course. Given that all the time points of HepG2/C3A 3D spheroid culture in this study clearly separated into three groups, we performed a K-means clustering (Watanabe, 2022) with a K value of 4 (the way that k=4 was chosen described in Methods). The top 2000 genes were broken down into four clusters based on similar gene expression dynamics patterns over the time-course where expression of cluster 1 and cluster 2 genes are initially decreased, while genes in cluster 3 and cluster 4 follow the opposite pattern at the transition from 2D to Day 3 in spheroid culture (Fig. 4A). During the transition from Day 10 to Day 14, cluster 1 genes maintained decreased gene expression, while cluster 2 exhibited increased gene expression (Fig. 4A). Cluster 3 genes showed decreased expression levels at the transition, while cluster 4 maintained increased gene expression from the initial transition point (Fig. 4A). The levels of gene expression of cluster 3 and cluster 4 genes increased immediately after formation of HepG2/C3A spheroids, which suggests biologically important roles of those genes in spheroid functionality. Further pathway enrichment analysis (KEGG and GO-BP) was carried out for these clusters to test for enrichment of specific biological pathways (Fig. 4B and Fig. S9). In cluster 3, a common enriched pathway resulting from both KEGG pathway and GO-BP term enrichment analysis included cell growth-related pathways. Terms such as DNA replication, cell cycle, and chromatin assembly were among the top 10 pathways enriched in the analysis using both databases. These enrichment results suggest that gene expression changes in genes within cluster 3 reflect changes in cell growth-related genes (Fig. 4B and Fig. S9A). Notably, the gene expression dynamics pattern of cluster 3 genes (cell growth-related genes) correlated to the observed pattern of change in cell doubling time, which showed a noticeable increase (decreased rate of cell growth) during the

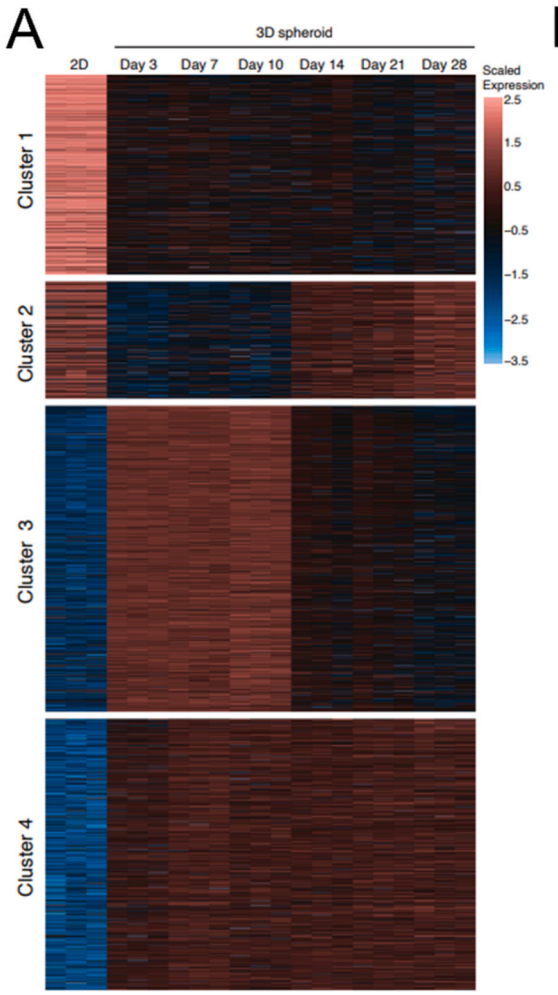






(caption on next page)

Fig. 3. Whole-transcriptome changes during 3D spheroid culture compared to 2D monolayer control. (A) PCA plot of all time points of 3D spheroid culture. The x-axis indicates PC1 that explains 77 % of variation in all samples while the y-axis indicates PC2 that explains 18 % of variation in all samples. (B) An intersection plot visually presenting the number of common and unique genes with greater expression in each time points during the 3D spheroid culture compared to 2D culture. Black dots represent the unique genes of each time point and a black line connecting the dots indicates a common set of unique genes. For instance, 1284 (the first blue bar graph value) indicates the number of common genes with greater expression in all time points in the spheroid culture as depicted by the connected line among black dots. (C) Top five enriched GO (biological pathway) terms of 1284 common up-regulated DEGs (shown in B) in all time points of 3D spheroid culture as compared to 2D monolayer control.



B

Cluster	P-adj.	KEGG Enriched Pathway
1	1.16E-07	MAPK signaling pathway
	6.44E-06	Regulation of actin cytoskeleton
	9.20E-05	Focal adhesion
	2.78E-03	Axon guidance
	2.78E-03	Glycosaminoglycan biosynthesis - chondroitin sulfate
	3.78E-03	Cytokine-cytokine receptor interaction
	5.87E-03	Leukocyte transendothelial migration
2	4.25E-04	Prion diseases
	1.11E-02	Primary bile acid biosynthesis
	1.69E-02	Steroid hormone biosynthesis
	1.69E-02	Nitrogen metabolism
3	1.84E-27	Systemic lupus erythematosus
	3.94E-22	**Cell cycle**
	9.01E-12	**DNA replication**
	2.78E-08	**Homologous recombination**
	2.25E-07	Oocyte meiosis
	1.55E-05	Progesterone-mediated oocyte maturation
	2.23E-05	Steroid biosynthesis
4	2.07E-14	Complement and coagulation cascades
	1.51E-10	Glycine, serine and threonine **metabolism**
	5.16E-08	**Drug metabolism - cytochrome P450**
	3.88E-07	PPAR signaling pathway
	1.72E-06	Glycolysis / Gluconeogenesis
	4.23E-06	**Metabolism of xenobiotics by cytochrome P450**
	2.48E-04	Fatty acid **metabolism**
	6.07E-04	Glutathione **metabolism**
	7.01E-04	Alanine, aspartate and glutamate **metabolism**
	8.55E-04	Butanoate **metabolism**

Fig. 4. Expression pattern-based clustering of genes and time points of HepG2/C3A 3D spheroid culture and enriched pathways of each cluster. (A) A heatmap (normalized and mean-centered) resulting from K-means clustering (k=4). The x-axis represents time points of spheroid culture whereas the y-axis represents genes, and those genes were clustered. (B) The top 10 KEGG pathways enriched in each cluster of genes. P-adj.: False Discovery Rate (FDR)-adjusted p-value, Fold: fold-change.

transition from Day 10 to Day 14.

Among the top 10 KEGG pathways enriched in cluster 4 genes, 5 pathways are directly associated with metabolism (Glycine serine and threonine metabolism, Metabolic pathways, Drug metabolism-cytochrome P450, Metabolism of xenobiotics by cytochrome P450, and Cholesterol metabolism) (Fig. 4B). Complementary GO enrichment analysis further revealed that the dominant GO-BP terms in cluster 4 were related to metabolism, with 9 out of 10 terms associated with metabolic pathways (Fig. S9B). Thus, these results are consistent with increased mRNA expression of a large number of genes encoding metabolism-related pathways at the initial formation of spheroids and their increased expression remains throughout the time-course of spheroid culture until Day 28. In summary, the overall view of gene expression dynamics of HepG2/C3A 3D spheroid culture using the K-means clustering approach also revealed two distinct transitions in time points: 2D / Day 3, 7, and 10 / Day 14, 21, and 28. Four clusters of genes with different gene expression dynamics and distinct enriched biological pathways showed concordance with these transition points.

3.5. Cell proliferation-related gene expression pattern showed a critical transition from Day 10 to Day 14

We further investigated DEGs between the Day 10 and Day 14 time points where we noted the change in growth characteristics and gene expression dynamics. We found that many genes encoding proteins involved in DNA replication and cell cycle pathways, both of which are critical for cell growth and proliferation, undergo a clear transition in gene expression levels with markedly decreased expression between Day 10 and Day 14 (Fig. 5). Among the DNA replication genes, the mini-chromosome maintenance (MCM) family, including MCM2, MCM3, MCM4, MCM5, MCM6, and MCM7, showed decreased expression levels during the transition (Fig. 5A). The MCM proteins encoded by this gene

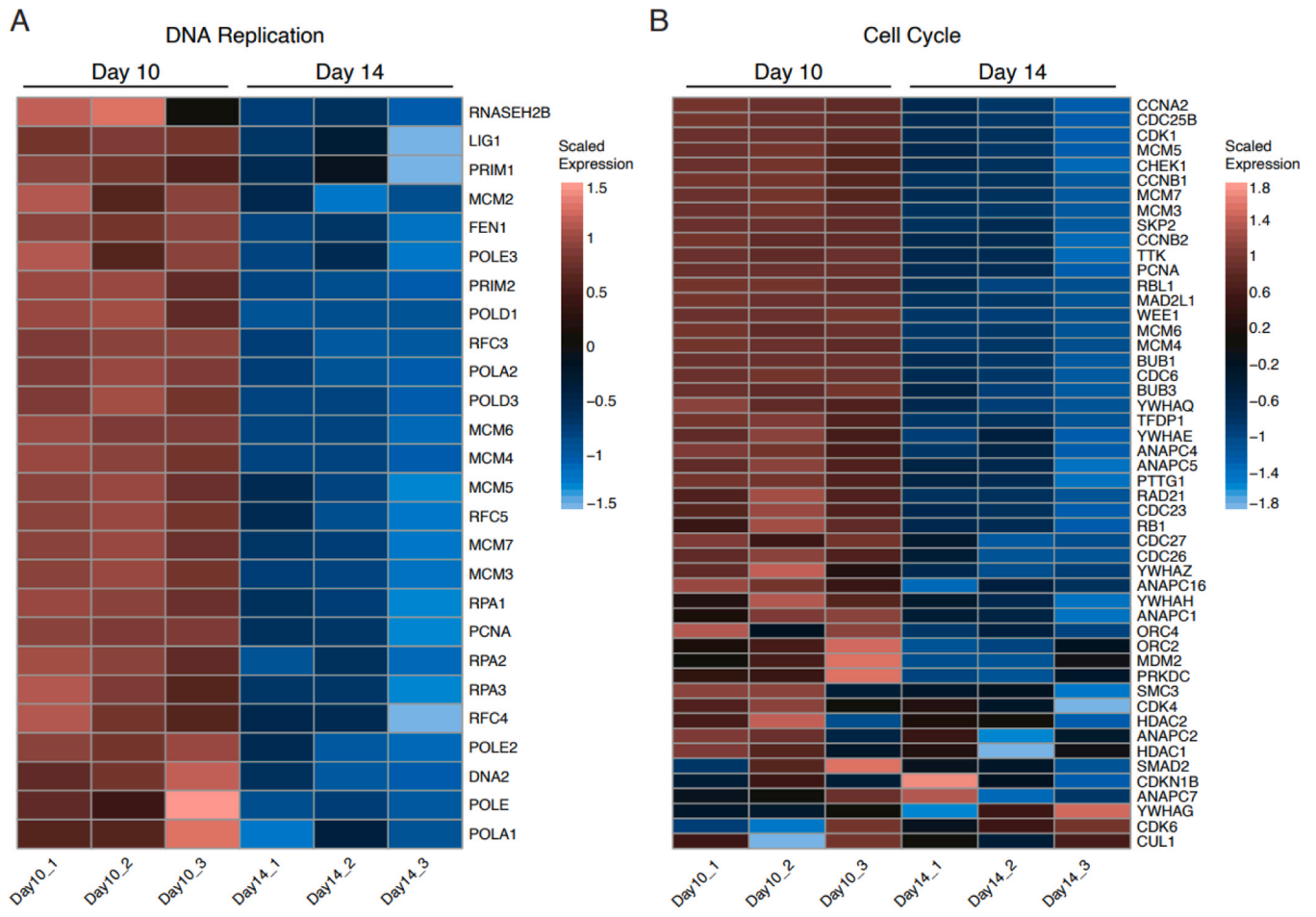


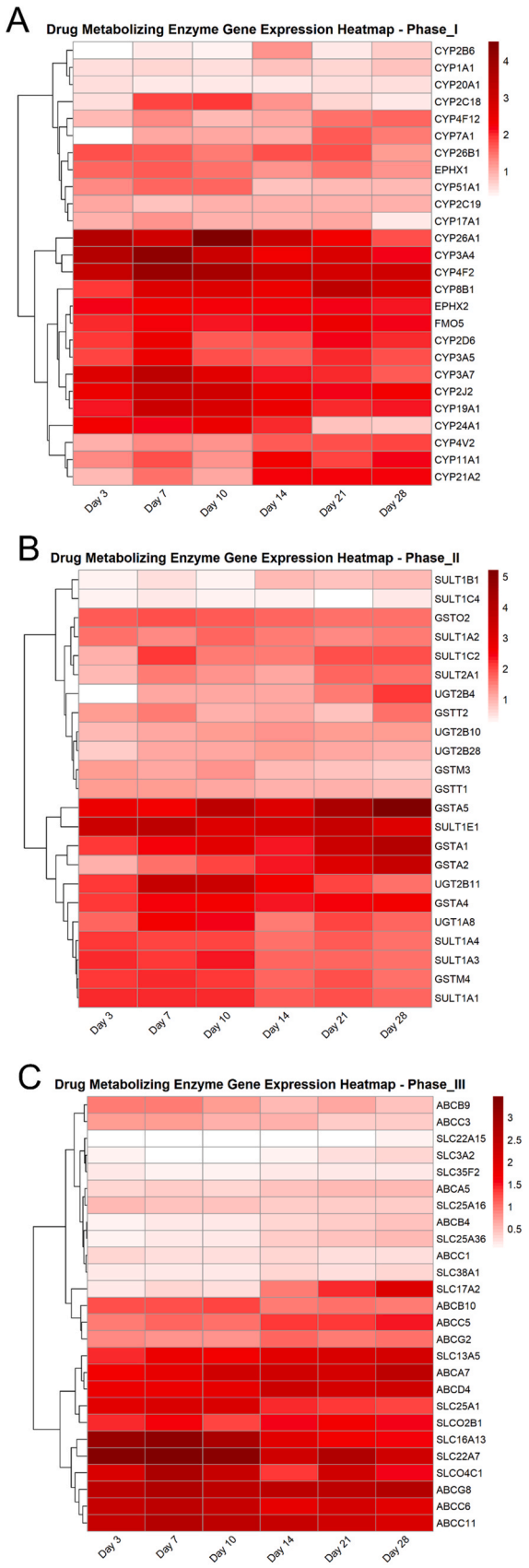
Fig. 5. Changes in cell proliferation-related gene expression during the transition point from Day 10 to Day 14 in spheroid culture. (A) A heatmap presents a list of genes involved in DNA replication pathway (KEGG) by visualizing changes in gene expression level using red (up-regulation) and blue (down-regulation). (B) A heatmap presents a list of genes involved in cell cycle pathway (KEGG) by visualizing changes in gene expression level using red (up-regulation) and blue (down-regulation). Heatmaps were constructed with 'Day' on the x-axis and 'gene' on the y-axis. The red- and blue-colored parameters describing gene expression level changes were calculated based on direct comparison between gene expression value of Day 10 and that of Day 14.

family are known to be essential replication initiation factors and those genes are evolutionally conserved in all eukaryotes (Tye, 1999). Another evolutionarily well-conserved gene, the proliferating cell nuclear antigen (PCNA), which plays critical roles in multiple processes of DNA replication (Moldovan et al., 2007), also showed decreased expression (Fig. 5A). The set of genes highlighted in green (indicating decreased expression levels) in the corresponding KEGG pathway (Supplementary Figure S8A) visually indicates that most of the genes involved in the DNA replication process undergo decreased expression. Cell-cycle genes also followed the same trend of gene expression dynamics as DNA replication genes (Fig. 5B). For example, essential cell division cycle regulators (Perbal, 2018) (cyclin A2 (CCNA2) and cyclin B1 (CCNB1)) showed decreased expression when spheroid culture transitioned from Day 10 to Day 14. Cyclin-dependent kinase 1 (CDK1) also showed a similar change in expression, which is expected since it has been shown to be activated by cyclins (Kalous et al., 2020). This trend of gene expression dynamics was also reflected in the corresponding KEGG pathway (Supplementary Figure S8B). Overall, the majority of genes involved in cell growth and proliferation pathways (DNA replication and cell cycle) have undergone a transition in their gene expression towards decreased expression levels.

3.6. *Drug metabolizing gene expression dynamics*

We observed a systematic increase in the expression of metabolism-related genes and pathways at all time points during HepG2/C3A 3D spheroid culture as compared to 2D controls (Fig. 3 and Fig. 4), but also noted that expression of metabolism pathway-related genes (arbitrarily separated into "Phase I, II, and III") fluctuated over the time course. We present the mean normalized expression (Median normalization method, refer to Methods section) with standard error of the mean (SEM) in Table S2 of selected Phase I, II, and III genes. This depiction is meant to be representative and not necessarily comprehensive to provide insight into their gene expression dynamics. Importantly, the HepaG2/C3A models expressed only a subset of these genes known to be expressed in primary human liver hepatocytes (Bell et al., 2016; Kvist et al., 2018). We included in Phase I, all cytochrome P450 (CYP) genes found to have significant expression levels in this cell model, as well as epoxide hydrolase (EH, EPHX), and flavin-containing monooxygenase (FMO). The gene families of glutathione S-transferase (GST), UDP-glycosyltransferase (UGT), and sulfotransferase (SULT) were selected for phase II DMEs. Finally, ATP-binding cassette (ABC) transporters, solute carriers (SLC) transporters, and solute carrier organic onion (SLCO) transporters were selected as representing phase III DMEs. The normalized gene expression values were then visualized in a heatmap to present an overview of their changes over time (Fig. 6). In comparison to the 2D control (the relative expression level was scaled to be equal to '1'), the overall expression level across the different categories was increased in the spheroid culture at all-time points.

Interestingly, some metabolism related genes showed similar gene



(caption on next column)

Fig. 6. Heatmap displaying overall gene expression pattern of drug metabolizing enzyme encoding genes summarized in Table S2. Individual drug/toxicant metabolizing enzyme/transporter genes categorized by Phase I (A), Phase II (B), and Phase III (C), are listed in the y-axis while time points are indicated in the x-axis. The values in the heatmap are the log ratios of the mean normalized gene expression for each time-point divided by the mean normalized gene expression of the 2D control samples. Thus, the changes in gene expression are relative to the baseline 2D control values.

expression dynamics patterns as the cell proliferation genes, with an early increase in expression from Day 3 to Day 10 and subsequent decrease in gene expression after Day 10. To obtain more insights into how the expression of metabolism related genes fluctuate during spheroid culture, a Trendy (Bacher et al., 2018) analysis, which is based on segmented regression modeling, was performed for the selected metabolism related genes summarized in Table S2 (Figs. 7A, 7C and Supplementary Fig. S4, S5, and S6). A few representative members from each phase are presented. Genes encoding cytochrome P450 enzymes (CYPs) (Zhao et al., 2021) showed several distinct trends in their gene expression change. For example, CYP3A4, CYP3A7, and CYP2J2 expression was increased at early time point (Day 3), peaked at Day 7, and then decreased after Day 10. Importantly, the normalized gene expression level at Day 3, Day 7, and Day 10 is always substantially elevated as compared to the 2D control, while that of Day 14, Day 21, and Day 28 is shown to be much less elevated (Figs. 7A, 7C, Supplementary Fig. S4). The gene expression dynamics of both CYP1A1 and CYP4V2 continuously increased until Day 28 although CYP1A1 differs in the extent of change, which appeared to be negligible compared to that of CYP4V2, which showed a robust increase over the time-course (Supplementary Fig. S4). CYP2D6 exhibited a dynamic pattern where there is no change in trend after Day 7, but immediate gene expression induction was observed on Day 3, and further on Day 7 (Supplementary Fig. S4). Other members of the phase I enzymes, such as EPHX and FMO showed a similar trend as CYPs with increased expression during all the time points of 3D spheroid culture (Supplementary Fig. S4).

For two CYPs, CYP3A4 and CYP1A1, we measured their time-course basal enzymatic activities up to Day 10 in spheroid cultures (the window where most pronounced gene expression changes were observed) and compared the results with 2D counterpart. CYP3A4 showed increase in enzymatic activity which matches its gene expression profile (Figs. 7A and 7B). In contrast, CYP1A1 gene expression showed an initial decrease in 3D culture as compared to 2D culture but enzymatic activity increased in 3D as compared to 2D culture despite decreased expression (Figs. 7C and 7D). Thus, changes in gene expression level and dynamics do not necessarily reflect the actual enzymatic activity of the corresponding genes.

Gene expression changes for four GST family genes, GSTT1, GSTM4, GSTO2, and GSTA1 were selected as representatives of the gene expression dynamics of phase II enzymes (Supplementary Fig. S5). They showed a similar trend where the expression level peaked at early time points (Day 3 or Day 7) and then decreased, except GSTA1, which increased its gene expression continuously until Day 28. SULTs and UGTs showed a similar pattern as GST family genes (Supplementary Fig. S5). Lastly, selected phase III transporters were investigated. ABCC6, ABCB10, and ABCG8 behaved similarly, presenting a dramatic decrease in gene expression as compared to 2D control on Day 3 in 3D culture (Supplementary Fig. S6). SLC transporters also follow the same trend where their gene expression peaked at Day 3 or Day 7 (Supplementary Fig. S6).

Most, but not all genes encoding DME (phase I, II, and III) showed a similar trend of gene expression dynamics during spheroid culture - dramatic early induction when transformed from 2D monolayer to 3D structure. Also, we found that most of the time points during the spheroid culture showed higher gene expression levels than the 2D monolayer control, regardless of their gene expression dynamics (Fig. 6 and Fig. 7), which implicates the recovery of metabolic competence in

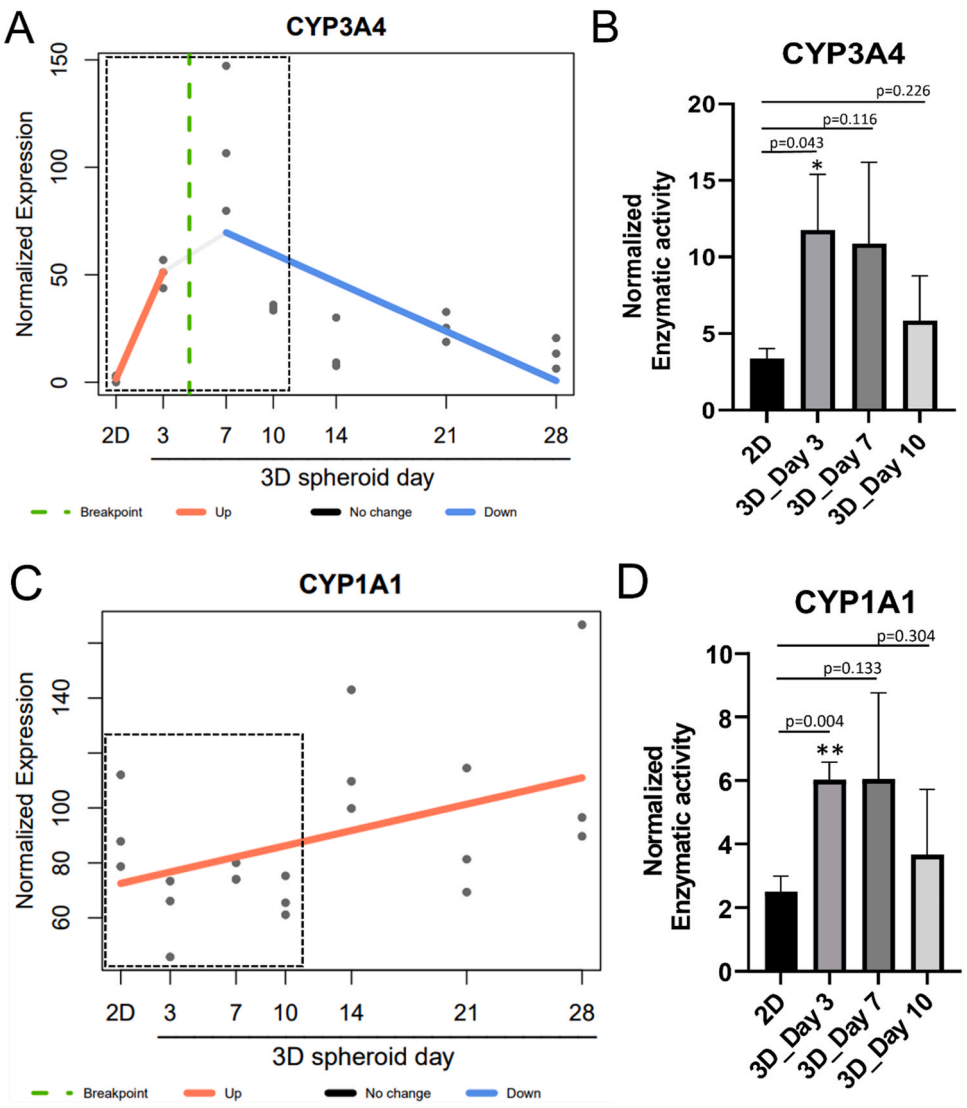


Fig. 7. Time-course gene expression change and corresponding enzymatic activity of representative Phase I enzymes. Trendy plots showing gene expression dynamics of CYP3A4 (A) and CYP1A1 (C). These plots are composed of gene name, x-axis, and y-axis. The x-axis indicates time in days while y-axis indicates normalized mRNA expression value. The grey dots in the same x-axis show individual normalized expression values of actual biological replicates. Green dotted line indicates a breakpoint where gene expression trend changes based on linear regression analysis by Trendy. The red line indicates 'up' trend of gene expression dynamics whereas the blue line indicates 'down' trend. The black line depicts no statistically significant change in trend of gene expression. Normalized enzymatic activities of CYP3A4 (B) and CYP1A1 (D) in 2D and 3D spheroid cultures (up to Day 10) were presented. *p-value <0.05; **p-value <0.01. The assays were performed in three replicates.

3D spheroids at least regarding the DME gene expression.

4. Discussion

The development of *in vitro* human cell model systems for assessing the potential toxicity of chemicals to human hepatocytes that balance high throughput capabilities, ease of use, and metabolic competence remains an ongoing challenge (Guillouzo, 1998; Allen et al., 2005; Bandele et al., 2012). Primary human hepatocytes (PHH) while the most metabolically active and representative of fully differentiated cells, can be challenging to culture, short lived and not amendable to genetic modifications (Guo et al., 2011; Gerets et al., 2012; Huggett et al., 2022). iPSC-derived hepatocytes are still challenging to culture and differentiate into fully mature adult hepatocytes (Corbett and Duncan, 2019). Tumor derived cell lines such as HepG2, while extensively utilized in toxicology due to ease of culture and rapid proliferation, are reported to have limited metabolic capacity (Arzumanian et al., 2021). Some tumor derived cell lines such as HepaRG can be induced to differentiate into hepatocyte-like cells with more organotypic phenotypes than HepG2 cells (Gerets et al., 2012; Nelson et al., 2017; Lőrincz et al., 2021) and increased metabolic activity (Dubois-Pot-Schneider et al., 2022; Louisse et al., 2023), but concerns about HepaRG cancerous features (Gupta et al., 2021) remain. More recently, HepG2/C3A cells, a derivative of HepG2, are being considered for their utility in toxicity studies due to their more differentiated and metabolically active hepatic phenotype compared to its original counterpart, HepG2 cells (Coltman et al., 2021). HepG2/C3A cells cultured in 3D spheroids recover some hepatocyte functions such as storage of glycogen, transport of bile salts, and the formation of structures resembling bile canaliculi (Okamoto et al., 2009; Ramaiahgari et al., 2014; Skolik et al., 2021). Furthermore, studies comparing whole-genome expression of HepG2 and HepaRG in chemical hazard identification capability concluded that HepG2 is more suitable for discriminating different genotoxic compounds using toxicogenomic approaches (Bhattacharya et al., 2005; Jennen et al., 2010; Magkoufopoulou et al., 2011). Moreover, high metabolic capacity and CYP inducibility, measured by gene expression or enzyme activity, do not necessarily correlate with high sensitivity for the detection of hepatotoxic drugs (Gerets et al., 2012; Bell et al., 2016). More recently,

according to Basharat et al., HepG2/C3A spheroids showed a higher sensitivity in response to a list of drug induced liver injury (DILI)--causing chemicals than HepaRG spheroids, demonstrating a superior predictiveness of HepG2/C3A in evaluating the early DILI responses in drug development (Basharat et al., 2020). These studies suggest that HepG2/C3A spheroids may be an appropriate model for comparative studies of differential molecular responses and phenotypes to chemical exposures. We thus undertook a detailed assessment of HepG2/C3A cells cultured in a spheroid cell model to ascertain its suitability for subsequent genotype-phenotype based studies.

A clinostat principle-based 3D culture system (ClinoStar, CelVivo) has recently been adopted to generate 3D spheroids for use in numerous studies in toxicology, stem cell biology, and virus pathology(Calitz et al., 2018; Štampar et al., 2021; Frandsen et al., 2022; Stewart et al., 2022; Pinzón-Arteaga et al., 2023) due to potential benefits over other 3D systems, including high uniformity in size, active diffusion of oxygen and nutrients, and mitigation of gravitational forces and shear stress. This system supports uniform spheroid maintenance for long-term culture periods as compared to other 3D systems, such as scaffold (collagen or matrigel)-based, hanging drop, or magnetic levitation (Haycock, 2011; Ramaiahgari et al., 2014; Langhans, 2018). We utilized this clinostat system to maintain HepG2/C3A spheroids and assess the phenotypic and gene expression in long term culture. As documented in the Fig. 2, spheroids were able to grow in a highly consistent manner over time up to 35 days.

Spheroids with a diameter above 500 μm (Nath and Devi, 2016) are reported to develop a “necrotic” core, which has been attributed to decreased diffusion of oxygen and nutrients from the culture media into the center of spheroid as it increases in size, as well as the accumulation of metabolic waste products. Interestingly, the cellular phenotypic results (Fig. 2) showed that the average diameter of the spheroids reaches 500 μm shortly before Day 10, the approximate transition time point at which the rate of cell proliferation and cell doubling dramatically decrease. Limited nutrient and oxygen exchange is consistent with the decreased in cell proliferation observed in our study. This phenomenon was also observed in Fig. 2C, where ATP production in cells appeared to slightly decrease compared to cell numbers consistent with hypoxic conditions negatively affects cell metabolism and energy distribution (Flood et al., 2023). The presence of a nutrient and oxygen gradient has been argued to better mimic the cellular heterogeneity of liver tissue and translatability (Zanoni et al., 2016). Such heterogeneity stems from large spheroids characterized by an external proliferating zone and internal quiescent zone (Zanoni et al., 2016), where the majority of cells experience hypoxia and glucose starvation that can be present in actual tissues (Wrzesinski and Fey, 2018). Nonetheless, the use of large spheroid models composed of cells in different proliferative and metabolic states has raised concerns about the reproducibility of data (Zanoni et al., 2016), which required careful interpretation of the data obtained in later timepoints regarding the quality of data. The HepG2/C3A spheroids generated and cultivated in this study started showing a darker core consistent with a necrotic core observed in a previous study (Štampar et al., 2020) from Day 14 and gene expression showed a transition around Day 10. Thus, the determination of the appropriate time window for toxicity studies in this system will depend on the question of interest. Exposure prior to Day 10 may be appropriate for high-throughput toxicant screening to reduce heterogeneity in response while later exposures may provide a more the heterogenous response mimicking complex tissue structures.

In previous studies (Wrzesinski and Fey, 2013; Wrzesinski et al., 2013), the cellular growth rate of individual cells comprising spheroids was assessed by measuring the protein content of a spheroid using photomicrograph-based estimation. The estimated cell doubling time, calculated indirectly using protein content, exceeded 12 days (288 hours) around the14th day of spheroid culture (Wrzesinski and Fey, 2013). In our study, we used cell-number (cell counting)-based doubling time calculation to obtain more precise data on cellular growth and avoid over- or underestimation by measuring protein content. 10 spheroids were collected at each timepoint which showed consistent measurements and low variation. Furthermore, we validated the cell counting data with an ATP-based cell proliferation assay which showed a high correlation (Fig. 2C). Comparing our direct measurement of two cell growth parameters (ATP-based cell proliferation assay and cell counting) with the previous protein-based estimation, the cell doubling time differed significantly, with our study finding significantly slower doubling time of 74 hours on Day 14 (Fig. 2D), approximately one-third of the value (240 hours) reported in the previous study (Wrzesinski and Fey, 2013; Wrzesinski et al., 2013). It is not clear what accounts for the significant difference in the doubling time estimates but does suggest that the doubling rate may be underestimated using the protein-based doubling time measurement. It is possible that the observed differences could arise from the different cell densities of each spheroid in a bioreactor, which might cause differences in oxygen and nutrient uptake by individual cells (Browning et al., 2021), potentially altering cell growth over the culture period. According to our results, we identified a pronounced transition time point where cell doublings change substantially, as indicated by our direct cell doubling measurement. The transition point in cell doubling provides important information for specific applications using HepG2/C3A spheroid models in toxicology as well as other applications, such as in tissue engineering and regenerative medicine development (Heydari et al., 2020).

Targeted and genome-wide transcriptomics in the field of toxicology has enabled profiling of transcriptional signatures in response to chemical exposures, utilizing whole animal, tissue, or cell culture models. This approach can identify transcriptionally regulated biological pathways that can help in the identification of mechanisms of toxicity (van Delft et al., 2012; Bushel et al., 2018; Zheng et al., 2018; Haimbaugh et al., 2022). We investigated the dynamics of the whole-transcriptome in HepG2/C3A 3D spheroids to establish a baseline for toxicological studies using this system. Xenobiotic exposure have been primarily addressed in 2D systems, with a focus on early detection of molecular phenotypes associated with toxic effects (Baccarelli and Bollati, 2009; Joseph, 2017). In addition to providing information on basal gene expression dynamics, our analysis revealed an enrichment of differentially expressed genes (increased expression levels) related to metabolism pathways at all time points during spheroid culture compared to 2D systems. This finding confirms several previous studies reporting increased expression levels of genes involved in metabolism processes (either gene expression or enzyme activity) when human liver cell lines form spheroids (Ramaiahgari et al., 2017; Wrzesinski and Fey, 2018; Eilenberger et al., 2019; Mandon et al., 2019; Štampar et al., 2020, 2021; Kanebratt et al., 2021; Rose et al., 2022). Surprisingly, we observed extensive changes in gene expression levels after 3 days of culture as spheroids, and these significant molecular alterations persisted throughout the entire spheroid culture period. This result appears to contrast with some previous reports documenting that HepG2/C3A spheroids recover physiological competence (metabolic capacity) after 18 days in 3D culture (Wrzesinski and Fey, 2013; Wrzesinski et al., 2013). Although factors associated with liver-like properties, such as bile duct formation and albumin expression (Bell et al., 2016; Ardisasmita et al., 2022), may also contribute to physiological relevance, our finding of immediate improvements (induction) in metabolism pathways can inform optimal exposure time windows during HepG2/C3A spheroid culture.

In general, changes in cellular phenotypes are often closely associated with molecular phenotype, such as changes in gene expression, loss of protein stability, alterations in enzymatic activity, and modifications of protein-protein, protein-DNA, or protein-ligand interactions (Rao et al., 2014; Wierbowski et al., 2018; Cozzolino et al., 2021; Lee et al., 2023). Although not establishing a causal link (Lin and Musunuru, 2018), gene expression-based molecular phenotypes can provide information about the genes or transcriptional networks which drive changes in cellular phenotypes of interest. DEGs between adjacent time points in

the study clearly indicated transitions in mRNA expression levels over the culture period which could influence response to external stimuli. The large number of DEGs when comparing 2D cultured cells and the early Day 3 spheroids, as well as the additional DEGs noted when comparing Day 10 and Day 14 spheroids, suggests significant functional changes in specific biological pathways occurred between these time points (Fig. S7 and Fig. 4). PCA plot and clustering analyses also demonstrated a clear separation of time points, supporting the finding of DEGs between adjacent time points. Moreover, the enriched KEGG and GO pathways in genes in cluster 3 from K-means clustering identified cell cycle and DNA replication processes, which are the pathways directly related to cell proliferation. These time-course analyses using whole-transcriptome (molecular phenotype) data are consistent with a time-course change in cell doubling time (cellular phenotype) shown in Fig. 2.

Since the absence or lower expression levels of some key drug-metabolizing enzymes are considered a significant issue with the HepG2/C3A cells (Guo et al., 2011), we assessed the gene expression of a set of genes encoding drug-metabolizing enzymes, including selected phase I, phase II, and phase III enzymes. The activity and inducibility of CYP enzymes (Phase I) are important determinants of the pharmacokinetics and toxicity of drugs/chemicals; thus, poor expression of these enzymes in hepatic cell lines is considered a key factor in the inaccurate prediction of toxicity in humans (Ramaiahgari et al., 2014). The overall trend of gene expression levels of most CYPs and other drug-metabolizing enzymes were shown to be higher in the spheroid model as compared to the 2D control (Fig. 6 and Fig. 7), consistent with the result of the K-means clustering analysis where metabolism-related genes and pathways were increased in spheroids as compared to 2D. Although the absolute expression levels of metabolic enzymes are generally lower in HepG2 /C3A than in other liver *in vitro* models, such as HepaRG and hepatocyte-like cells (HLCs) (Ardisasmita et al., 2022), our results suggest a rapid enhancement of metabolic capacity in spheroid cultures as compared to the 2D counterpart. Furthermore, we showed that gene expression dynamics of two representative CYPs, CYP3A4 and CYP1A1, are not always correlated with actual enzymatic activities as shown in Fig. 7. While CYP3A4 showed a good correlation between gene expression (increased) and enzymatic activity (increased) in spheroid cultures, CYP1A1 showed increase enzymatic activity upon spheroid formation whereas gene expression didn't increase upon spheroid formation. CYP3A4 basal enzymatic activity in HepG2 spheroids has been examined, with reports ranging from three- to seven-fold increases compared to 2D counterpart which is aligned with our data (Yang et al., 2013; Sun et al., 2024).

Of note, the basal whole-transcriptome dynamics and cellular growth rate along the time-course culture in HepG2/C3A spheroids investigated in this study could potentially provide informative insights for establishing a particular *in vitro* model that maintains cellular proliferation while achieving improved metabolic capacity. For example, there have been growing demands and efforts to utilize 3D cell culture models for functional genetic screens (i.e., targeted or genome wide CRISPR screen in spheroid models) to identify important genetic factors involved in cellular responses to environmental cues or stimulations in a more physiologically relevant condition (Takahashi et al., 2020; Zhang et al., 2022; Meng et al., 2023). Such approaches have found that tumor cells in 3D culture are largely dependent on NRF2 hyperactivation (Takahashi et al., 2020), prostate cancer cells treated with PARPi drugs are enriched with novel genetic components involved in DNA repair pathways (Zhang et al., 2022), and neurodevelopment disorders (NDDs) genes are responsible for human interneuron development (Meng et al., 2023). However, these studies have not considered cell doubling times in 3D culture which could confound the interpretation of results. Furthermore, it is also important to investigate the critical time window for appropriate exposure to toxicants in spheroid-based studies. The data in this study, including the cell doublings data in combination with the gene expression dynamics of drug-metabolizing enzymes, suggests that a time window from Day 3 to Day 10 is appropriate exposure period for use in a proliferation-based 3D spheroid CRISPR screen in HepG2/CA3. The combined cellular and molecular phenotypic data can be practically used to select balanced and optimal experimental conditions necessary for 3D genetic screens approach using HepG2/C3A in the future.

5. Conclusions

In this study, HepG2/C3A spheroids were successfully generated and cultivated for 35 days (5 weeks) using the CelVivo bioreactor system based on the clinostat principle. We profiled the whole-transcriptome changes of the spheroids to comprehensively inform the baseline molecular phenotypic changes during 3D culture using the TempO-Seq platform. With a particular focus on cellular growth and metabolic capacity (expression of genes encoding drug metabolism enzymes), we report several findings, some of which are consistent with previous studies while others are novel.

CRediT authorship contribution statement

Zhaohan Zhu: Writing – review & editing, Visualization, Software, Methodology, Formal analysis, Data curation. **Christopher D. Vulpe:** Writing – review & editing, Supervision, Project administration, Investigation, Funding acquisition, Conceptualization. **Rhonda L. Bacher:** Writing – review & editing, Visualization, Supervision, Software, Project administration, Methodology, Funding acquisition, Formal analysis, Conceptualization. **W. Brad Barbazuk:** Writing – review & editing, Supervision, Project administration, Funding acquisition, Conceptualization. **Chanhee Kim:** Writing – review & editing, Writing – original draft, Visualization, Validation, Software, Methodology, Investigation, Formal analysis, Data curation, Conceptualization.

Declaration of Competing Interest

The authors declare that they have no known competing financial interests or personal relationships that could have appeared to influence the work reported in this paper.

Data Availability

Data will be made available on request.

Acknowledgements

This study was supported by NIEHS (the grant number is R01ES033625).

Appendix A. Supporting information

Supplementary data associated with this article can be found in the online version at doi:10.1016/j.toxlet.2024.10.004.

References

Adams, J.C., 2019. A new initiative for AJP-cell physiology: "making cell culture more physiological. " *Am. J. Physiol. -Cell Physiol. 316*, C828–C829. https://doi.org/10.1152/ajpcell.00157.2019.

Allen, D.D., Caviedes, R., Cárdenas, A.M., et al., 2005. Cell lines as in vitro models for drug screening and toxicity studies. Drug Dev. Ind. Pharm. *31*, 757–768. https://doi.org/10.1080/03639040500216246.

Anders, S., Huber, W., 2010. Differential expression analysis for sequence count data. Genome Biol. *11*, R106. https://doi.org/10.1186/gb-2010-11-10-r106.

Ardisasmita, A.I., Schene, I.F., Joore, I.P., et al., 2022. A comprehensive transcriptomic comparison of hepatocyte model systems improves selection of models for experimental use. Commun. Biol. *5*, 1–15. https://doi.org/10.1038/s42003-022-04046-9.

Arzumanian, V.A., Kiseleva, O.I., Poverennaya, E.V., 2021. The Curious Case of the HepG2 Cell Line: 40 Years of Expertise. Int J. Mol. Sci. 22, 13135. https://doi.org/10.3390/ijms222313135.

Baccarelli, A., Bollati, V., 2009. Epigenetics and environmental chemicals. Curr. Opin. Pedia *21*, 243–251. https://doi.org/10.1097/mop.0b013e32832925cc.
Bacher, R., Leng, N., Chu, L.-F., et al., 2018. Trendy: segmented regression analysis of expression dynamics in high-throughput ordered profiling experiments. BMC Bioinforma. *19*, 380. https://doi.org/10.1186/s12859-018-2405-x.
Bandele, O.J., Santillo, M.F., Ferguson, M., et al., 2012. In vitro toxicity screening of chemical mixtures using HepG2/C3A cells. Food Chem. Toxicol. https://doi.org/10.1016/j.fct.2012.02.016. Accessed May 24, 2023].
Barisam, M., Saidi, M.S., Kashaninejad, N., et al., 2018. Prediction of Necrotic Core and Hypoxic Zone of Multicellular Spheroids in a Microbioreactor with a U-Shaped Barrier. Micromachines *9*, 94. https://doi.org/10.3390/mi9030094.
Basharat, A., Rollison, H.E., Williams, D.P., et al., 2020. HepG2 (C3A) spheroids show higher sensitivity compared to HepaRG spheroids for drug-induced liver injury (DILI). Toxicol. Appl. Pharm. *408*, 115279. https://doi.org/10.1016/j.taap.2020.115279.
Bell, C.C., Hendriks, D.F.G., Moro, S.M.L., et al., 2016. Characterization of primary human hepatocyte spheroids as a model system for drug-induced liver injury, liver function and disease. Sci. Rep. *6*, 25187. https://doi.org/10.1038/srep25187.
Bhattacharya, B., Cai, J., Luo, Y., et al., 2005. Comparison of the gene expression profile of undifferentiated human embryonic stem cell lines and differentiating embryoid bodies. BMC Dev. Biol. *5*, 22. https://doi.org/10.1186/1471-213X-5-22.
Browning, A.P., Sharp, J.A., Murphy, R.J., et al., 2021. Quantitative analysis of tumour spheroid structure. eLife *10*, e73020. https://doi.org/10.7554/eLife.73020.
Bushel, P.R., Paules, R.S. and Auerbach, S.S. (2018). A Comparison of the TempO-Seq S1500+ Platform to RNA-Seq and Microarray Using Rat Liver Mode of Action Samples. *Front Genet 9*. DOI: 10.3389/fgene.2018.00485.
Calitz, C., Hamman, J.H., Viljoen, A.M., et al., 2018. Toxicity and anti-prolific properties of Xysmalobium undulatum water extract during short-term exposure to two-dimensional and three-dimensional spheroid cell cultures. Toxicol. Mech. Methods *28*, 641–652. https://doi.org/10.1080/15376516.2018.1485805.
Coltman, N.J., Coke, B.A., Chatzi, K., et al., 2021. Application of HepG2/C3A liver spheroids as a model system for genotoxicity studies. Toxicol. Lett. *345*, 34–45. https://doi.org/10.1016/j.toxlet.2021.04.004.
Corbett, J.L., Duncan, S.A., 2019. iPSC-derived hepatocytes as a platform for disease modeling and drug discovery. Front Med *6*. https://doi.org/10.3389/fmed.2019.00265.
Cox, J.A., Fellows, M.D., Hashizume, T., et al., 2016. The utility of metabolic activation mixtures containing human hepatic post-mitochondrial supernatant (S9) for in vitro genetic toxicity assessment. Mutagenesis *31*, 117–130. https://doi.org/10.1093/mutage/gev082.
Cozzolino, F., Iacobucci, I., Monaco, V., et al., 2021. Protein–DNA/RNA interactions: an overview of investigation methods in the -omics Era. J. Proteome Res *20*, 3018–3030. https://doi.org/10.1021/acs.jproteome.1c00074.
van Delft, J., Gaj, S., Lienhard, M., et al., 2012. RNA-seq provides new insights in the transcriptome responses induced by the carcinogen Benzo[a]pyrene. Toxicol. Sci. *130*, 427–439. https://doi.org/10.1093/toxsci/kfs250.
Deisenroth, C., DeGroot, D.E., Zurlinden, T., et al., 2020. The alginate immobilization of metabolic enzymes platform retrofits an estrogen receptor transactivation assay with metabolic competence. Toxicol. Sci. J. Soc. Toxicol. 178, 281–301. https://doi.org/10.1093/toxsci/kfaa147.
Dubois-Pot-Schneider, H., Aninat, C., Kattler, K., et al., 2022. Transcriptional and epigenetic consequences of DMSO treatment on HepaRG cells. Cells *11*, 2298. https://doi.org/10.3390/cells11152298.
Eilenberger, C., Rothbauer, M., Ehmoser, E.-K., et al., 2019. Effect of spheroidal age on sorafenib diffusivity and toxicity in a 3D HepG2 spheroid model. Sci. Rep. *9*, 4863. https://doi.org/10.1038/s41598-019-41273-3.
Flecknell, P., 2002. Replacement, reduction, and refinement. ALTEX *19*, 73–78. ⟨https://www.altex.org/index.php/altex/article/view/1106⟩.
Flood, D., Lee, E.S., Taylor, C.T., 2023. Intracellular energy production and distribution in hypoxia. J. Biol. Chem. 299, 105103. https://doi.org/10.1016/j.jbc.2023.105103.
Fontana, F., Marzagalli, M., Sommariva, M., et al., 2021. In Vitro 3D Cultures to Model the Tumor Microenvironment. Cancers *13*, 2970. https://doi.org/10.3390/cancers13122970.
Frandsen, H.S., Vej-Nielsen, J.M., Smith, L.E., et al., 2022. Mapping proteome and lipidome changes in early-onset non-alcoholic fatty liver disease using hepatic 3D spheroids. Cells *11*, 3216. https://doi.org/10.3390/cells11203216.
Gaidatzis, D., Lerch, A., Hahne, F., et al., 2015. QuasR: quantification and annotation of short reads in R. Bioinformatics *31*, 1130–1132. https://doi.org/10.1093/bioinformatics/btu781.
Ge, S.X., Son, E.W., Yao, R., 2018. iDEP: an integrated web application for differential expression and pathway analysis of RNA-Seq data. BMC Bioinforma. *19*, 534. https://doi.org/10.1186/s12859-018-2486-6.
Gerets, H.H.J., Tilmant, K., Gerin, B., et al., 2012. Characterization of primary human hepatocytes, HepG2 cells, and HepaRG cells at the mRNA level and CYP activity in response to inducers and their predictivity for the detection of human hepatotoxins. Cell Biol. Toxicol. *28*, 69–87. https://doi.org/10.1007/s10565-011-9208-4.
Guillouzo, A., 1998. Liver cell models in in vitro toxicology. Environ. Health Perspect. *106* (*Suppl 2*), 511–532. https://doi.org/10.1289/ehp.98106511.
Guo, L., Dial, S., Shi, L., et al., 2011. Similarities and differences in the expression of drug-metabolizing enzymes between human hepatic cell lines and primary human hepatocytes. Drug Metab. Dispos. *39*, 528–538. https://doi.org/10.1124/dmd.110.035873.
Gupta, R., Schrooders, Y., Hauser, D., et al., 2021. Comparing in vitro human liver models to in vivo human liver using RNA-Seq. Arch. Toxicol. *95*, 573–589. https://doi.org/10.1007/s00204-020-02937-6.
Haimbaugh, A., Meyer, D., Akemann, C., et al., 2022. Comparative toxicotranscriptomics of single cell RNA-seq and conventional RNA-Seq in TCDD-exposed testicular tissue. Front Toxicol. *4*. https://doi.org/10.3389/ftox.2022.821116.
Harrill, J.A., Everett, L.J., Haggard, D.E., et al., 2021. High-throughput transcriptomics platform for screening environmental chemicals. Toxicol. Sci. J. Soc. Toxicol. *181*, 68–89. https://doi.org/10.1093/toxsci/kfab009.
Haycock, J.W., 2011. 3D Cell Culture: A Review of Current Approaches and Techniques. In: Haycock, In.J.W. (Ed.), 3D Cell Culture. Humana Press, Totowa, NJ, pp. 1–15. https://doi.org/10.1007/978-1-60761-984-0_1.
Heydari, Z., Najimi, M., Mirzaei, H., et al., 2020. Tissue engineering in liver regenerative medicine: insights into novel translational technologies. Cells *9*, 304. https://doi.org/10.3390/cells9020304.
Hirsch, H.R., Engelberg, J., 1965. Determination of the cell doubling-time distribution from culture growth-rate data. J. Theor. Biol. 9, 297–302. https://doi.org/10.1016/0022-5193(65)90114-1.
House, J.S., Grimm, F.A., Klaren, W.D., et al., 2022. Grouping of UVCB substances with dose-response transcriptomics data from human cell-based assays. *ALTEX 39*, 388–404. https://doi.org/10.14573/altex.2107051.
Huggett, Z.J., Smith, A., De Vivo, N., et al., 2022. A Comparison of Primary Human Hepatocytes and Hepatoma Cell Lines to Model the Effects of Fatty Acids, Fructose and Glucose on Liver Cell Lipid Accumulation. Nutrients *15*, 40. https://doi.org/10.3390/nu15010040.
Jennen, D.G.J., Magkoufopoulou, C., Ketelslegers, H.B., et al., 2010. Comparison of HepG2 and HepaRG by whole-genome gene expression analysis for the purpose of chemical hazard identification. Toxicol. Sci. *115*, 66–79. https://doi.org/10.1093/toxsci/kfq026.
Joseph, P., 2017. Transcriptomics in toxicology. Food Chem. Toxicol. Int J. Publ. Br. Ind. Biol. Res Assoc. *109*, 650–662. https://doi.org/10.1016/j.fct.2017.07.031.
Kalous, J., Jansová, D., Šušor, A., 2020. Role of cyclin-dependent kinase 1 in translational regulation in the M-phase. Cells *9*, 1568. https://doi.org/10.3390/cells9071568.
Kanebratt, K.P., Janefeldt, A., Vilén, L., et al., 2021. Primary human hepatocyte spheroid model as a 3D in vitro platform for metabolism studies. J. Pharm. Sci. *110*, 422–431. https://doi.org/10.1016/j.xphs.2020.10.043.
Kvist, A.J., Kanebratt, K.P., Walentinsson, A., et al., 2018. Critical differences in drug metabolic properties of human hepatic cellular models, including primary human hepatocytes, stem cell derived hepatocytes, and hepatoma cell lines. Biochem Pharm. 155, 124–140. https://doi.org/10.1016/j.bcp.2018.06.026.
Langhans, S.A., 2018. Three-dimensional in vitro cell culture models in drug discovery and drug repositioning. Front Pharm. *9*. https://doi.org/10.3389/fphar.2018.00006.
Lee, J.J., Ramadesikan, S., Black, A.F., et al., 2023. Heterogeneity in lowe syndrome: mutations affecting the phosphatase domain of OCRL1 differ in impact on enzymatic activity and severity of cellular phenotypes. Biomolecules *13*, 615. https://doi.org/10.3390/biom13040615.
Li, C.-L., Tian, T., Nan, K.-J., et al., 2008. Survival advantages of multicellular spheroids vs. monolayers of HepG2 cells in vitro. Oncol. Rep. *20*, 1465–1471. https://doi.org/10.3892/or_00000167.
Lilienblum, W., Dekant, W., Foth, H., et al., 2008. Alternative methods to safety studies in experimental animals: role in the risk assessment of chemicals under the new European Chemicals Legislation (REACH). Arch. Toxicol. *82*, 211–236. https://doi.org/10.1007/s00204-008-0279-9.
Lin, J., Musunuru, K., 2018. From genotype to phenotype: a primer on the functional follow-up of genome-wide association studies in cardiovascular disease. Circ. Genom. Precis Med *11*, e001946. https://doi.org/10.1161/CIRCGEN.117.001946.
Lőrincz, T., Deák, V., Makk-Merczel, K., et al., 2021. The performance of HepG2 and HepaRG systems through the glass of acetaminophen-induced toxicity. Life *11*, 856. https://doi.org/10.3390/life11080856.
Louisse, J., Fragki, S., Rijkers, D., et al., 2023. Determination of in vitro hepatotoxic potencies of a series of perfluoroalkyl substances (PFASs) based on gene expression changes in HepaRG liver cells. Arch. Toxicol. *97*, 1113–1131. https://doi.org/10.1007/s00204-023-03450-2.
Love, M.I., Huber, W., Anders, S., 2014. Moderated estimation of fold change and dispersion for RNA-seq data with DESeq2. Genome Biol. *15*, 550. https://doi.org/10.1186/s13059-014-0550-8.
Magkoufopoulou, C., Claessen, S.M.H., Jennen, D.G.J., et al., 2011. Comparison of phenotypic and transcriptomic effects of false-positive genotoxins, true genotoxins and non-genotoxins using HepG2 cells. Mutagenesis *26*, 593–604. https://doi.org/10.1093/mutage/ger021.
Mandon, M., Huet, S., Dubreil, E., et al., 2019. Three-dimensional HepaRG spheroids as a liver model to study human genotoxicity in vitro with the single cell gel electrophoresis assay. Sci. Rep. *9*, 10548. https://doi.org/10.1038/s41598-019-47114-7.
Meng, X., Yao, D., Imaizumi, K., et al., 2023. Assembloid CRISPR screens reveal impact of disease genes in human neurodevelopment. Nature *622*, 359–366. https://doi.org/10.1038/s41586-023-06564-w.
Mišík, M., Nersesyan, A., Ropek, N., et al., 2019. Use of human derived liver cells for the detection of genotoxins in comet assays. Mutat. Res Toxicol. Environ. Mutagen *845*, 402995. https://doi.org/10.1016/j.mrgentox.2018.12.003.
Moldovan, G.-L., Pfander, B., Jentsch, S., 2007. PCNA, the maestro of the replication fork. Cell *129*, 665–679. https://doi.org/10.1016/j.cell.2007.05.003.
Nath, S., Devi, G.R., 2016. Three-dimensional culture systems in cancer research: Focus on tumor spheroid model. Pharm. Ther. *163*, 94–108. https://doi.org/10.1016/j.pharmthera.2016.03.013.
Nelson, L.J., Morgan, K., Treskes, P., et al., 2017. Human hepatic HepaRG cells maintain an organotypic phenotype with high intrinsic CYP450 activity/metabolism and significantly outperform standard HepG2/C3A cells for pharmaceutical and

therapeutic applications. Basic Clin. Pharm. Toxicol. *120*, 30–37. https://doi.org/10.1111/bcpt.12631.
Okamoto, T., Kanemoto, N., Ban, T., et al., 2009. Establishment and characterization of a novel method for evaluating gluconeogenesis using hepatic cell lines, H4IIE and HepG2. Arch. Biochem Biophys. *491*, 46–52. https://doi.org/10.1016/j.abb.2009.09.015.
Pamies, D., Hartung, T., 2017. 21st century cell culture for 21st century toxicology. Chem. Res Toxicol. *30*, 43–52. https://doi.org/10.1021/acs.chemrestox.6b00269.
Perbal, B., 2018. The concept of the CCN protein family revisited: a centralized coordination network. J. Cell Commun. Signal *12*, 3–12. https://doi.org/10.1007/s12079-018-0455-5.
Pinto, B., Henriques, A.C., Silva, P.M.A., et al., 2020. Three-dimensional spheroids as in vitro preclinical models for cancer research. Pharmaceutics *12*, 1186. https://doi.org/10.3390/pharmaceutics12121186.
Pinzón-Arteaga, C.A., Wang, Y., Wei, Y., et al., 2023. Bovine blastocyst-like structures derived from stem cell cultures. Cell Stem Cell *30*, 611–616.e7. https://doi.org/10.1016/j.stem.2023.04.003.
Ramaiahgari, S.C., den Braver, M.W., Herpers, B., et al., 2014. A 3D in vitro model of differentiated HepG2 cell spheroids with improved liver-like properties for repeated dose high-throughput toxicity studies. *Arch. Toxicol.* https://doi.org/10.1007/s00204-014-1215-9.
Ramaiahgari, S.C., Waidyanatha, S., Dixon, D., et al., 2017. From the cover: three-dimensional (3D) HepaRG spheroid model with physiologically relevant xenobiotic metabolism competence and hepatocyte functionality for liver toxicity screening. Toxicol. Sci. *159*, 124–136. https://doi.org/10.1093/toxsci/kfx122.
Rao, V.S., Srinivas, K., Sujini, G.N., et al., 2014. Protein-protein interaction detection: methods and analysis. Int J. Proteom. *2014*, 147648. https://doi.org/10.1155/2014/147648.
Richardson, S.J., Bai, A., Kulkarni, A.A., et al., 2016. Efficiency in drug discovery: liver S9 fraction assay as a screen for metabolic stability. Drug Metab. Lett. *10*, 83–90. https://doi.org/10.2174/1872312810666160223121836.
Robinson, A.T., Cook, M.D., Lane-Cordova, A.D., 2020. Making cell culture more physiological: a call for a more comprehensive assessment of racial disparities in endothelial cell culture studies. Am. J. Physiol. Cell Physiol. *318*, C238–C241. https://doi.org/10.1152/ajpcell.00467.2019.
Rose, S., Cuvellier, M., Ezan, F., et al., 2022. DMSO-free highly differentiated HepaRG spheroids for chronic toxicity, liver functions and genotoxicity studies. Arch. Toxicol. *96*, 243–258. https://doi.org/10.1007/s00204-021-03178-x.
Rowan-Carroll, A., Reardon, A., Leingartner, K., et al., 2021. High-throughput transcriptomic analysis of human primary hepatocyte spheroids exposed to per- and polyfluoroalkyl substances as a platform for relative potency characterization. Toxicol. Sci. *181*, 199–214. https://doi.org/10.1093/toxsci/kfab039.
Schmeisser, S., Miccoli, A., von Bergen, M., et al., 2023. New approach methodologies in human regulatory toxicology – not if, but how and when! Environ. Int *178*, 108082. https://doi.org/10.1016/j.envint.2023.108082.
Singh, S., Khanna, V.K., Pant, A.B., 2018. Chapter 1 - development of in vitro toxicology: a historic story. In: Dhawan, A., Kwon, S. (Eds.), In Vitro Toxicology. Academic Press. https://doi.org/10.1016/B978-0-12-804667-8.00001-8.
Skolik, R.A., Solocinski, J., Konkle, M.E., et al., 2021. Global changes to HepG2 cell metabolism in response to galactose treatment. Am. J. Physiol. -Cell Physiol. *320*, C778–C793. https://doi.org/10.1152/ajpcell.00460.2020.
Soldatow, V.Y., LeCluyse, E.L., Griffith, L.G., et al., 2012. In vitro models for liver toxicity testing. Toxicol. Res *2*, 23–39. https://doi.org/10.1039/C2TX20051A.
Štampar, M., Breznik, B., Filipič, M., et al., 2020. Characterization of in vitro 3D cell model developed from human hepatocellular carcinoma (HepG2) cell line. Cells *9*, 2557. https://doi.org/10.3390/cells9122557.
Štampar, M., Sedighi Frandsen, H., Rogowska-Wrzesinska, A., et al., 2021. Hepatocellular carcinoma (HepG2/C3A) cell-based 3D model for genotoxicity testing of chemicals. Sci. Total Environ. *755*, 143255. https://doi.org/10.1016/j.scitotenv.2020.143255.
Štampar, M., Tomc, J., Filipič, M., et al., 2019. Development of in vitro 3D cell model from hepatocellular carcinoma (HepG2) cell line and its application for genotoxicity testing. Arch. Toxicol. *93*, 3321–3333. https://doi.org/10.1007/s00204-019-02576-6.
Stewart, R., Yan, K., Ellis, S. et al. (2022). Increased neurovirulence of omicron BA.5 and XBB variants over BA.1 in K18-hACE2 mice and human brain organoid. https://doi.org/10.1101/2022.12.22.521696.
Stokes, W.S., 2015. Animals and the 3Rs in toxicology research and testing: the way forward. Hum. Exp. Toxicol. *34*, 1297–1303. https://doi.org/10.1177/0960327115598410.
Stransky, S., Cutler, R., Aguilan, J., et al., 2022. Investigation of reversible histone acetylation and dynamics in gene expression regulation using 3D liver spheroid model. Epigenetics Chromatin *15*, 35. https://doi.org/10.1186/s13072-022-00470-7.
Sun, B., Liang, Z., Wang, Y., et al., 2024. A 3D spheroid model of quadruple cell co-culture with improved liver functions for hepatotoxicity prediction. Toxicology 505, 153829. https://doi.org/10.1016/j.tox.2024.153829.
Takahashi, N., Cho, P., Selfors, L.M., et al., 2020. 3D culture models with CRISPR screens reveal hyperactive NRF2 as a prerequisite for spheroid formation via regulation of proliferation and ferroptosis. Mol. Cell *80*, 828–844.e6. https://doi.org/10.1016/j.molcel.2020.10.010.
Tye, B.K., 1999. MCM proteins in DNA replication. Annu Rev. Biochem *68*, 649–686. https://doi.org/10.1146/annurev.biochem.68.1.649.
Watanabe, N., 2022. A k-means method for trends of time series. Jpn J. Stat. Data Sci. *5*, 303–319. https://doi.org/10.1007/s42081-022-00148-0.
Wierbowski, S.D., Fragoza, R., Liang, S., et al., 2018. Extracting complementary insights from molecular phenotypes for prioritization of disease-associated mutations. Curr. Opin. Syst. Biol. *11*, 107–116. https://doi.org/10.1016/j.coisb.2018.09.006.
Wilkening, S., Stahl, F., Bader, A., 2003. Comparison of primary human hepatocytes and hepatoma cell line Hepg2 with regard to their biotransformation properties. Drug Metab. Dispos. *31*, 1035–1042. https://doi.org/10.1124/dmd.31.8.1035.
Wojdyla, K., Wrzesinski, K., Williamson, J., et al., 2016. Acetaminophen-induced S-nitrosylation and S-sulfenylation signalling in 3D cultured hepatocarcinoma cell spheroids. Toxicol. Res *5*, 905–920. https://doi.org/10.1039/c5tx00469a. ⟨https://doi.org/10.1039/c5tx00469a⟩.
Wrzesinski, K., Fey, S.J., 2013. After trypsinisation, 3D spheroids of C3A hepatocytes need 18 days to re-establish similar levels of key physiological functions to those seen in the liver. Toxicol. Res *2*, 123–135. https://doi.org/10.1039/c2tx20060k.
Wrzesinski, K., Fey, S.J., 2018. Metabolic reprogramming and the recovery of physiological functionality in 3D cultures in micro-bioreactors. Bioengineering *5*, 22. https://doi.org/10.3390/bioengineering5010022.
Wrzesinski, K., Frandsen, H.S., Calitz, C., et al., 2021. Clinostat 3D cell culture: protocols for the preparation and functional analysis of highly reproducible, large, uniform spheroids and organoids. Methods Mol. Biol. Clifton NJ 2273 17–62. https://doi.org/10.1007/978-1-0716-1246-0_2.
Wrzesinski, K., Magnone, M.C., Hansen, L.V., et al., 2013. HepG2/C3A 3D spheroids exhibit stable physiological functionality for at least 24 days after recovering from trypsinisation. Toxicol. Res *2*, 163–172. https://doi.org/10.1039/c3tx20086h.
Wrzesinski, K., Rogowska-Wrzesinska, A., Kanlaya, R., et al., 2014. The cultural divide: exponential growth in classical 2D and metabolic equilibrium in 3D environments. PloS One *9*, e106973. https://doi.org/10.1371/journal.pone.0106973.
Yang, Y., Li, J., Pan, X., et al., 2013. Co-culture with mesenchymal stem cells enhances metabolic functions of liver cells in bioartificial liver system. Biotechnol. Bioeng. 110, 958–968. https://doi.org/10.1002/bit.24752.
Yokoyama, Y., Sasaki, Y., Terasaki, N., et al., 2018. Comparison of drug metabolism and its related hepatotoxic effects in HepaRG, cryopreserved human hepatocytes, and HepG2 cell cultures. Biol. Pharm. Bull. *41*, 722–732. https://doi.org/10.1248/bpb.b17-00913.
Zanoni, M., Piccinini, F., Arienti, C., et al., 2016. 3D tumor spheroid models for in vitro therapeutic screening: a systematic approach to enhance the biological relevance of data obtained. Sci. Rep. *6*, 19103. https://doi.org/10.1038/srep19103.
Zhang, H., Gao, H., Gu, Y., et al., 2022. 3D CRISPR screen in prostate cancer cells reveals PARP inhibitor sensitization through TBL1XR1-SMC3 interaction. Front Oncol. *12*, 999302. https://doi.org/10.3389/fonc.2022.999302.
Zhao, M., Ma, J., Li, M., et al., 2021. Cytochrome P450 enzymes and drug metabolism in humans. Int J. Mol. Sci. *22*, 12808. https://doi.org/10.3390/ijms222312808.
Zheng, M., Lu, J., Zhao, D., 2018. Toxicity and transcriptome sequencing (RNA-seq) analyses of adult zebrafish in response to exposure carboxymethyl cellulose stabilized iron sulfide nanoparticles. Sci. Rep. *8*, 8083. https://doi.org/10.1038/s41598-018-26499-x.
Zobl, W., Bitsch, A., Blum, J., et al., 2023. Protectiveness of NAM-based hazard assessment – which testing scope is required? ALTEX - Alter. Anim. Exp. https://doi.org/10.14573/altex.2309081.